ORIGINAL PAPER

Biodegradable Conducting PVA-Hydrogel Based on Carbon Quantum Dots: Study of the Synergistic Effect of Additives

Jillian Gamboa[1,2] · Sofia Paulo-Mirasol[1,2] · Albert Espona-Noguera[2,3] · Hamidreza Enshaei[1,2] · Sergi Ortiz[1] · Francesc Estrany[1,2] · Maria-Pau Ginebra[2,3] · Juan Torras[1,2]

Abstract
Conductive hydrogels are becoming one of the most important milestones for the development of new scaffolds, biosensors, supercapacitors, and green electronics within the field of biomedicine. In this work, we study the effect of different types of electroactive additives such as poly(3,4-ethylenedioxythiophene), tannic acid, and carbon quantum dots (CQDs), to form different poly(vinyl alcohol) (PVA)-based hydrogels with enhanced electrochemical properties. Different physicochemical tests are carried out to characterize the different PVA-based hybrid hydrogels and the rates of their degradation and loss of electroactivity throughout an eight-week biodegradation process. This work shows the individual and synergistic effects of the additives on various mechanical properties, including storage modulus and swelling ratio, and electrochemical properties of the PVA hydrogel. The additives have proven to enhance the electroactivity of the PVA-based hydrogels but as well their degradation. Finally, the use of the new hydrogel as a pressure sensor is also investigated. The study provides an insight on the potential use of CQDs, in synergy with other electroactivity enhancers, in the fabrication of novel hybrid conducting hydrogels in green electronics.

Graphical Abstract
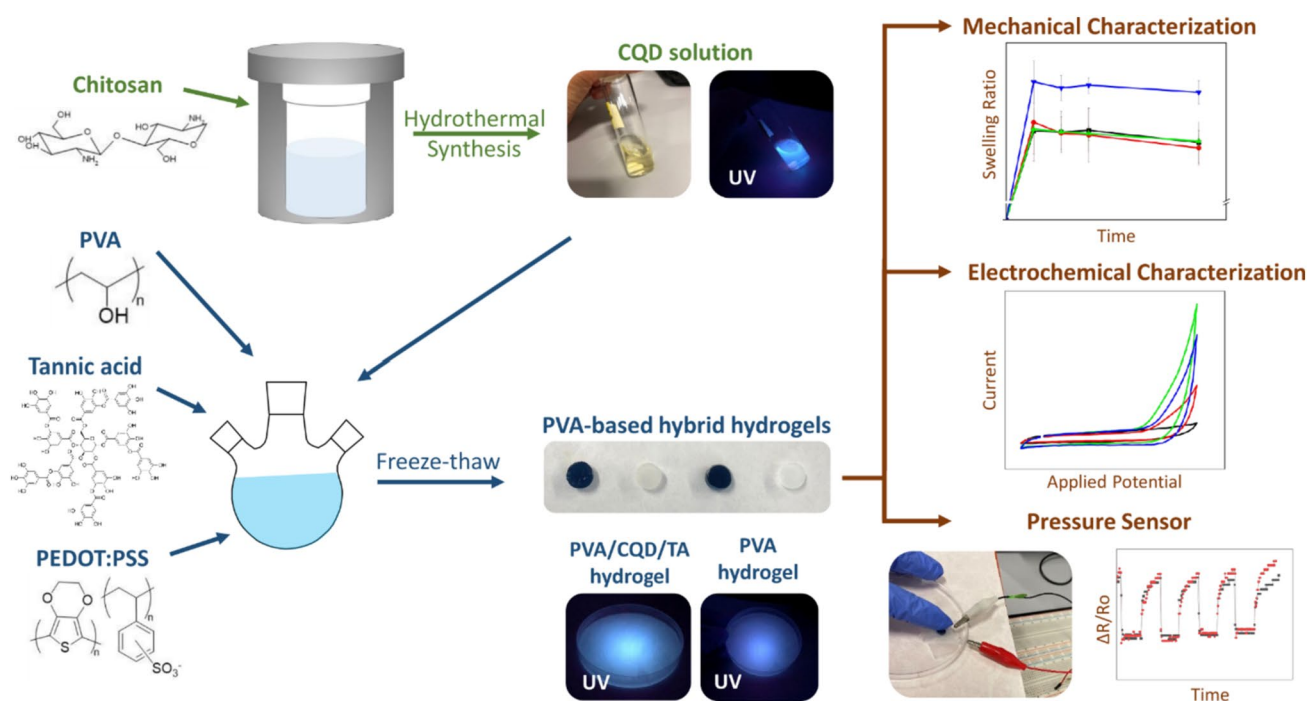
Extended author information available on the last page of the article

Introduction

Wearable electronic devices have become an element of everyday life. However, many of them have a very short lifespan which, together with their rapid development, results in an increase in electronic waste (e-waste), causing serious environmental pollution problems in their long degradation process [1]. In fact, the majority of e-waste in 2019 consisted of small equipment, including small medical devices and small monitoring and control instruments [2]. These concerns have encouraged researchers to develop new biosensing materials that are flexible, biocompatible, renewable, sustainable, and biodegradable for adaptation to complex environments when used in wearable electronics [3, 4]. Among the different biodegradable polymers extensively used, poly(vinyl alcohol) (PVA) stands out. PVA is a synthetic polymer that has sparked great interest in biomedical fields regarding its advantages such as biocompatibility, nontoxicity, biodegradability, hydrophilicity, and chemical stability. PVA can fully degrade into CO_2 and H_2O through microorganisms in soil and wastewater [5]. The most widespread applications of PVA for biomedical uses is in the hydrogel form, which is commonly fabricated through either physical or chemical methods. Physical crosslinking involves a set of cyclic thermal treatments of freezing-thawing (F-T cycles) where the formation of ice pushes PVA chains toward each other favoring the appearance of hydrogen bonds and the formation of crystalline domains. PVA domains are separated from the solid water phase, giving rise to a very porous material when the structural ice melts [6]. Chemical crosslinking involves aldehydes such as glutaraldehyde among others, with the ability to react with the free hydroxyl groups of different PVA chains. For biomedical applications, physical crosslinking has the advantage of tunable mechanical and diffusion properties as well as a larger biodegradability without the use of potentially harmful crosslinking agents [7].

PVA hydrogels lack intrinsic electrochemical properties, which are highly demanded in biomedical applications. However, due to its macroporous structure and its large number of hydroxyl groups located in the polymer chains, it can be easily combined with different materials with high electrochemistry, stabilized within the polymer matrix. Stable ionic conductivity can easily be acquired by integrating soluble metallic salts into the PVA hydrogel [8]. This can be combined with an increase in electrical conductivity by incorporating conductive materials (i.e., conductive nanoparticles [9], ionic liquids [10], conducting polymers [11], graphene [12], etc.). Indeed, electrochemically activated

PVA hydrogels, alone or in combination with other biomaterials, have been widely used in different applications such as biosensors [13], supercapacitors [14, 15], wound repair [16], water and energy harvesting [17] and soft electronics [18, 19], among others.

Recently, in the field of biomedicine and wearable devices, three additives among others, have aroused much attention and they are used to enhance the electrochemical and mechanical properties of hydrogels, i.e., poly(3,4-ethylenedioxythiophene):poly(styrenesulfonate) (PEDOT:PSS), tannic acid (TA), and carbon quantum dots (CQDs). PEDOT:PSS is a widely adopted conducting polymer for biomedical applications owing to its high biocompatibility and good electrochemical properties [20]. However due to its low mechanical strength, it is difficult to be used in flexible wearable devices. On the other hand, its combination with other more flexible materials improves its mechanical properties while improving electrochemical performance of the material in combination [21]. Liu et al. prepared a PVA/PEDOT:PSS hydrogel electrode for a flexible supercapacitor by the F-T crosslinking method showing a high porosity, stretchability, and compressibility, which was advantageous for enhancing the mechanical stability of the supercapacitor [22]. TA is a natural polyphenolic compound able to form multiple and strong hydrogen bonds with PVA. Beside its interesting crosslinking properties it also exhibits antioxidant, antibacterial and anti-inflammatory properties, which together with its electrochemical properties, becomes a promising additive for hydrogels, which has recently attracted much attention of researchers in the field of biomedicine [23, 24]. Finally, CQDs are a novel class of carbon-based nanomaterials with sizes lower than 10 nm (considered a zero-dimensional nanomaterial, 0D) with unique optical, electrochemical, biocompatibility, and photoluminescence (PL) properties. CQDs have graphite-like crystal lattices with a large number of surface functional groups, intrinsic state luminescence, and the quantum size confinement [25]. The polar chemical groups on the surface award CQDs high solubility in water and the possibility to act as building blocks in hydrogel formation, with the CQDs acting as cross-linkers, either through non-covalent interactions or reactions with additional gelling agents [26]. These properties make CQDs a promising material to be used as an electroactivity enhancer in hydrogels to be used in biomedicine [27–29].

Electroactive hydrogels, such as PVA-based conducting hydrogels are extremely useful in soft electronics and biomedicine [30]. In fact, there is a growing need for new

biomaterials with appropriate chemical, mechanical, and electrical properties that also have the ability to degrade over time so they can be eliminated from the body or from the environment following use. However, up to date, little attention has been paid to the stability of electrochemical enhanced PVA-hydrogels. In the development of new applications focused on the "green electronics" paradigm, the degradation not only of the material but also the corresponding loss of electrochemical properties will be a handicap to be taken into account in the future generations of materials [3]. Bannerman et al. demonstrated the ability of PVA loaded with iron oxide nanoparticles (NPs) to degrade over time and thus, to be used in drug delivery applications using stimuli-responsive hydrogels [31]. Similarly, Aragueta-Robles et al. showed that PVA-tyramine (PVA-tyr) system can be tuned to provide a soft degradable scaffold with mechanical properties matched to native neural tissue [32]. Recently, fabrication of fully bioresorbable, light, thin, flexible, and biocompatible supercapacitors has been reported, which are able to operate for 7 days in a liquid environment and fully degrade in vitro in 90 days without harming the environment [33].

In this work, we explored the use of three different electroactive additives (i.e., PEDOT:PSS, TA, and CQD) in a PVA hydrogel, physically crosslinked by cyclic FT process, to improve its electroactivity and mechanical properties. The analysis on the effect of additives is organized in two blocks, first the effect on the properties of each additive is studied independently and later the synergistic effect of several combined additives on the properties of the PVA-based hydrogel is discussed. Also, a degradation study is carried out with an emphasis on the electroactivity degradation, wherein the loss of mass and the changes in the specific capacitance (SC) are measured as indicators of the sample degradation. Finally, the best combination of PVA-based conductive hydrogels containing CQDs will be used as pressure sensors to show its applicability in green electronics and biomedicine.

Materials and Methods

Materials

Chitosan (M_W: 310–375 kDa), poly (vinyl alcohol) (PVA, M_W: 61 kDa and 98% degree of hydrolysis), tannic acid (TA), poly(3,4-ethylenedioxythiophene)-poly(styrenesulfonate) (PEDOT:PSS, 1.3% in water), acetonitrile (ACN), lithium perchlorate (LiClO$_4$), EDOT, and ITO-coated PET were purchased from Sigma Aldrich. Acetic acid (99.5%) was purchased from Avantor Sciences. Milli-Q water grade (0.055 µS/cm) was used in all the synthesis processes. Unless specified, all chemicals were used as received, without further modifications.

Synthesis of Carbon Quantum Dots

Carbon quantum dots were obtained following the method reported by Sun et al. (Fig. 1) [34]. Briefly, 0.1 g of chitosan was mixed with 20 mL of 1% acetic acid and vigorously stirred until the most of the chitosan has been dissolved. The remaining undissolved parts were removed through centrifugation at 11,000 rpm for 15 min. The supernatant was placed in a Teflon-lined stainless autoclave reactor and was kept in the heating block at 180 °C for at least 16 h. The reactor was cooled down naturally to room temperature. The resulting solution was centrifuged at 4000 rpm for 15 min and then filtered with a 22 µm filter to remove any debris from the reaction, resulting in a clear yellow solution. Finally, the solvent was evaporated and the remaining particles re-dispersed in Milli-Q water to obtain the desired concentration of 1% (w/w).

Hydrogels Preparation

PVA (98% degree of hydrolysis) was slowly added to Milli-Q water and stirred vigorously with a magnetic stirring bar while heated to 90 °C until all the PVA was dissolved and a homogeneous liquid phase was obtained. The PVA solution was cooled down to room temperature and placed in molds, which were then placed in −20 °C for 18–20 h and then in 4 °C for about 4–6 h. This freeze-thaw cycle was repeated three times. After the freeze thaw cycles, the hydrogels were washed in Milli-Q water three times and kept in Milli-Q water at 4 °C (Fig. 1).

For the hybrid hydrogels, the same procedure was followed but after cooling down of the PVA solution to room temperature, the additives solutions were slowly mixed in with the PVA solution for another hour to obtain a homogeneous mixture. The PVA solution (25% w/w), CQD (0.5% w/w), TA (20% w/w), and PEDOT:PSS (1.3% w/w) were mixed at various ratios. The final hydrogel composition for all synthesized composites are listed in the Table S1 (supporting information).

Chemical, Morphological and Electrochemical Characterization

Chemical Characterization

For the chemical characterizations of the hydrogels, Fourier transform infrared spectroscopy (FTIR) and Raman spectroscopy were performed. FTIR was performed using the Jasco 4100 spectrophotometer. For each sample, 64 scans were conducted between wavenumbers of 4000 and 600 cm^{-1}. Raman spectroscopy was performed using the Renishaw inVia Qontor
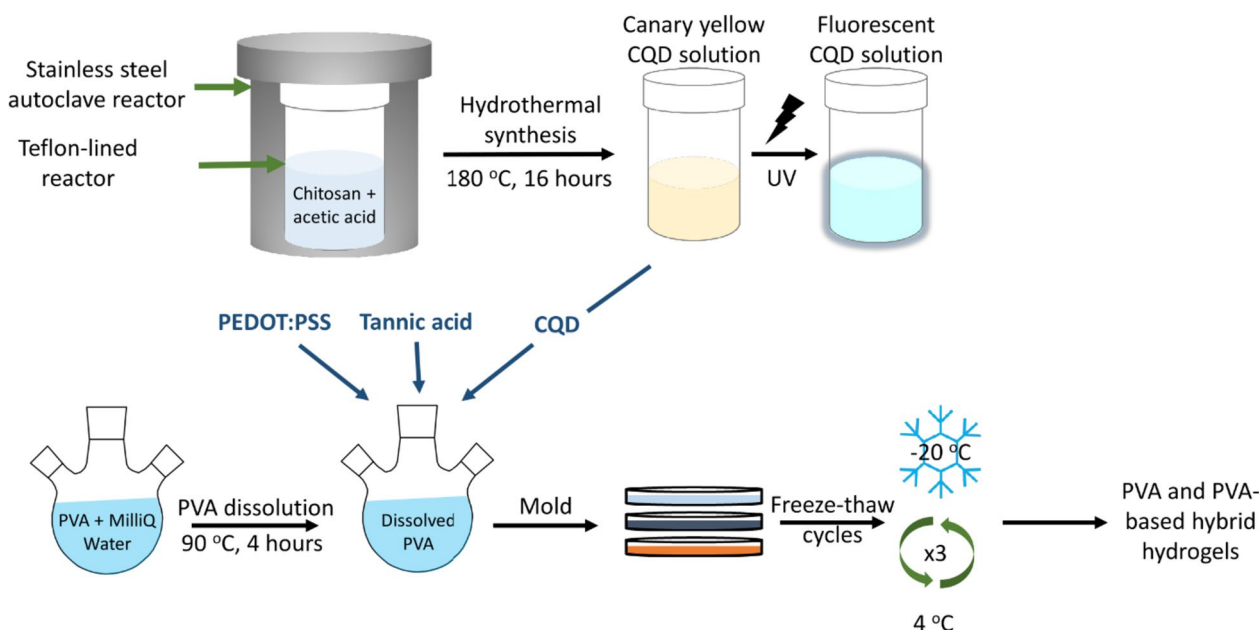
Fig. 1 A schematic of the synthesis of PVA-based conductive hydrogel. The initial highly hydrolyzed PVA polymer is solubilized and mixed with the electroactive enhancers prior to molding. The gelation process was achieved by physical crosslinking involving a set of cyclic freeze-thaw heat treatments to create final electroactive PVA hybrid hydrogels. CQDs fabrication is also shown

confocal Raman microscope. A laser of 785 nm was used with ten seconds of exposure time, 0.5% laser power, and 5 accumulations per sample.

Scanning Electron Microscopy

Scanning electron microscopy (SEM) was conducted for a detailed inspection of the samples. A Focused Ion Beam Zeis Neon 40 scanning electron microscope operating at 5 kV was used with a secondary electron detector to obtain the micrographs. The freeze-dried samples were supported onto a double-sided adhesive carbon disc and were sputter-coated with a thin layer of carbon to prevent sample charging problems using a K950X Turbo Evaporator.

Freeze-dried hydrogels were broken along the cross-section and analyzed under SEM. The images were then processed using the Image J software for pore size calculations.

Swelling Ratio

Lyophilized samples were placed in PBS buffer at pH 7.4 and placed in an incubator at 37 °C under constant stirring until the time for their characterization was reached, the swelled hydrogels were superficially dried and weighed. The swelling ratio (SR) was calculated using Eq. 1.

$$SR(\%) = \frac{w_{sn} - w_0}{w_0} \times 100 \tag{1}$$

wherein w_{sn} is the swelled weight of the hydrogel and w_0 is the initial lyophilized weight.

Electrochemical Characterization

Electrochemical characterization was performed using the Autolab PGSTAT204 controlled by the Nova software by means of cyclic voltammetry (CV). Pieces of the molded hydrogels (area = 25 mm^2, thickness = 2 mm) were cut out and patted with tissue paper to remove excess water. They were then placed between two sheets of poly(ethylene terephthalate) (PET) coated with indium titanium oxide (ITO), with the ITO sides facing the hydrogels. The sheets were then connected to the Autolab Potentiostat. CV measurements were performed at 100 mV s^{-1} between −0.1 to 1 V. Based on the CV results, specific capacitance (SC) was calculated using Eq. 2, where A is the area within the CV curve, k the scan rate, ΔV is the potential window in volts, and m is the mass of the freeze dried hydrogel sample in grams:

$$SC = \frac{A}{2\Delta Vkm} \tag{2}$$

The loss of electroactivity (LEA, in %) against the number of oxidation–reduction cycles was calculated using Eq. 3. This parameter will help to determine the electrochemical stability of the sample:

$$LEA = \frac{\Delta Q}{Q_3} = \frac{Q_3 - Q_i}{Q_3} x100 \tag{3}$$

where ΔQ is the difference between the oxidation charge (in C) of the third (Q_3) and the evaluated oxidation–reduction cycle (Q_i). Usually the first cycle at the experimental level is discarded, since a structural relaxation of the polymer that contains the hydrogel is always necessary, which takes place in the 1st and 2nd redox processes.

Electrochemical impedance spectroscopy (EIS) was also performed to test the conductivity of the hydrogels. For these tests, pieces of hydrogels (area = 25 mm², thickness = 2 mm) were soaked in 0.1 M NaCl solution overnight. The hydrogels were sandwiched between two stainless steel electrodes. The electrodes were first coated with a layer of PEDOT to improve the contact with the hydrogels. Electropolymerization of PEDOT was performed using 20 mM EDOT in 0.1 M LiClO$_4$ in acetonitrile under inert conditions. The electropolymerization time was adjusted to achieve a total charge of 300 mC cm^{-2}. The EIS measurements were performed by applying 50 mV from 0.1 to 10^5 Hz.

Rheological Evaluation

Oscillatory rheological experiments were conducted utilizing a Hybrid Rheometer Discovery HR-2 (TA Instruments) to determine the viscoelastic properties of all the hydrogels under study. The storage modulus (G') of disk-shaped hydrogels (diameter: 20 mm, thickness: 1 mm) was monitored during amplitude sweep measurements. To this end, samples were placed onto the rheometer platform, and then the amplitude sweep measurements ranging from 10^{-4} to 1 rad oscillatory displacements were performed at room temperature using the 20 mm parallel rugose plates configuration, at a frequency of 1 Hz, and a gap size of 500 μm. G' values determined at 10^{-3} rad displacement were used to compare all samples. At least, three independent experiments were conducted, each consisting of three replicates.

The axial compression test was performed using the same rheometer to determine the axial force required to induce a 25% deformation in all the studied hydrogels (hereafter, F_{ax25}). In this experiment disk-shaped hydrogels (diameter: 20 mm, thickness: 1 mm) were also employed, which were carefully placed onto the rheometer platform before measurements. Afterwards, the rheometer was set at compression mode with a constant motor linear rate of 16.67 μm s^{-1}, an angular velocity of 0 rad s^{-1}, and a sampling time of 0.1 s. At the point where the upper plate exerted an axial deformation of 25% with respect to the height of the sample, the applied axial force was measured. At least, three independent experiments were conducted, each consisting of three replicates.

Degradation Test

The hydrogel degradation test was conducted along 56 days (8 weeks) with all fabricated hybrid hydrogels by measuring the mass loss at intervals of 0, 1, 3, 7, 14, 21, 27, 56 days. In all cases, 6 different samples per time point were used, 3 samples for the swelling and degradation ratio, and another 3 samples for the specific capacitance measurement. The different hybrid hydrogels previously manufactured and molded in large pieces were divided into small portions and lyophilized for 72 h for later weighing. Each of the freeze-dried samples was placed inside an Eppendorf tube with a PBS solution (pH 7.4) and subjected to constant stirring at 37 °C in an incubator to proceed with the degradation test. At each desired degradation time point, the samples were washed three times in Milli-Q water to remove any salts and then lyophilized for a second time to obtain the degraded weight. The degradation ratio (DR) was calculated using the following equation:

$$DR(\%) = \frac{w_0 - w_n}{w_0} \times 100 \tag{4}$$

wherein, w_0 is the initial lyophilized weight of the sample and w_n is the lyophilized weight of the sample at degradation time point n.

To test the electrochemical activity loss during degradability study, the samples used for electrochemical characterization were not subjected to any prior or subsequent lyophilization but a direct CV tests were performed at each desired degradation time point.

Pressure Tests

Pieces of two hybrid hydrogels (PVA/CQD/TA and PVA/PEDOT/CQD/TA) with diameters of 8 mm and thicknesses of 3 mm were cut out. The superficial water was dried out and the sample placed between two ITO-coated PET sheets, which were then connected to an Arduino Mega 2560 microprocessor. A voltage input of 3.3 V was supplied to the circuit and a program was created to measure the resistance of the sample with and without pressure. The set was used to measure the relative resistance change ($\Delta R/R_0$) as described in Eq. 5, where R_r is the real-time resistance and R_0 is the original resistance without any external loading.

$$\frac{\Delta R}{R_0}(\%) = \frac{R_r - R_0}{R_0} \times 100 \tag{5}$$

Results and Discussion

Carbon Quantum Dots Characterization

Nitrogen CQDs were prepared using the hydrothermal method previously proposed by Sun et al. [34]. Morphological analysis of these CQDs previously reported, was showing an uniform particle-size average of 1.94 nm [29]. As-prepared CQDs were subsequently characterized using spectroscopic techniques. Figure 2a shows the UV–VIS absorption spectrum of the CQDs with a peak absorbance at 285 nm. Also, the PL was measured at different excitation wavelengths (Fig. 2b). The spectra show that the CQDs obtained present the highest PL count at an excitation wavelength of 340 nm with an emission wavelength of 410 nm. These results are in agreement with the previous study carried out by Sun et al. [34].

ATR-FTIR measurements of powder nitrogen CQDs were conducted (Fig. 2c). FTIR shows a strong peak centered at 3200 cm^{-1}, which belongs to the stretching vibration of O−H and N−H. The peaks at 1648 cm^{-1},

1575 cm^{-1}, and 1397 cm^{-1} can be attributed to the stretching vibration of C=O, C=C, and C–N, respectively. The peaks at 2928 cm^{-1}, 1299 cm^{-1}, and 875 cm^{-1} can be ascribed to the stretching and bending vibrations of C−H bond. The peak at 1015 cm^{-1} represents the characteristic peak of C−O stretching vibration. The results also confirm the presence of –COOH, −NH$_2$, and –OH moieties, which could form hydrogen bonds with the PVA chains that could enhance the entrapment of the CQDs within the PVA hydrogel [34, 35] and as well as attribute to good hydrophilicity of the CQDs.

Enhancement of Mono-additive PVA-Based Hydrogel Properties

Electrochemical Effect

Different additives (i.e., PEDOT:PSS, TA and CQDs) were considered to improve the mechanical and electrical properties of the PVA hydrogel. Initially, a study was carried out on the effect of the electroactivity of each additive used, both individually mixed with the PVA hydrogel matrix and

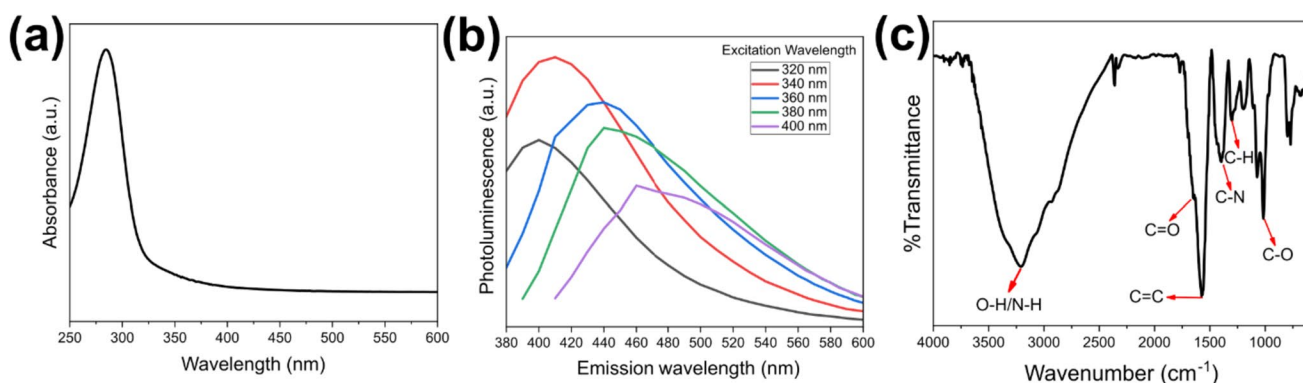**Fig. 2** **a** UV–Vis absorbance spectrum of CQDs. **b** The photoluminescence spectra of CQDs at different light excitation wavelengths. **c** FTIR spectrum of CQDs
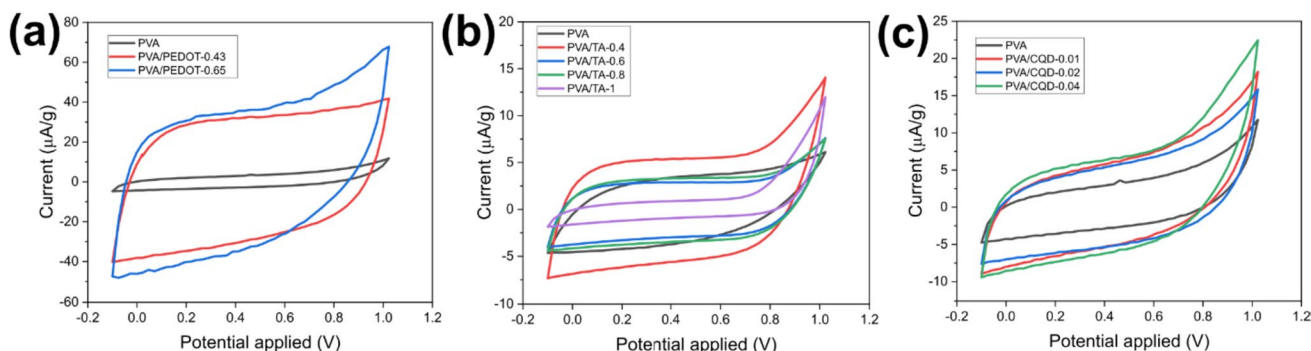
Fig. 3 Cyclic voltammograms at cycle 3 for **a** PVA/PEDOT, **b** PVA/TA and **c** PVA/CQD hydrogels. Voltammograms were obtained at the scan rate of 50 mV s^{-1} using aqueous solutions with different concentrations of PEDOT, TA, and CQD

in solution. Figure 3 shows the CVs of PVA/PEDOT, PVA/TA and PVA/CQD hydrogels at different additive concentrations. CVs were performed via solid state 2-electrode system at a scan rate of 50 mV s^{-1} and using fresh hydrogels swelled in Milli-Q water. PEDOT:PSS led to an increase in the CV area, indicating an increase in the electroactivity of the hydrogel (Fig. 3a). Thus obtaining a maximum specific capacitance (SC) of 0.50 mF g^{-1} in the PVA/PEDOT-0.65 hydrogel. Both additives, TA and CQDs present electroactivity as observed in Figure S1 with a similar SC values of 2.14 and 1.69 mF g^{-1} for a solution of TA and CQD, respectively. TA is expected to also confer additional mechanical properties to the final hydrogel due to the hydrogen bonds formation between the alcohol and carbonyl groups of both components, which will stabilize PVA crosslinking [24]. In agreement with the results of the CV of TA in solution, the addition of TA to the hydrogel also resulted in an increase in the peak oxidation current and as well as an increase in the area of the CV curve (Fig. 3b), demonstrating that the addition of TA also improved the electroactivity of the hydrogel. However, upon increasing the concentration of TA in the hydrogel, a decrease in CV area was observed. This could indicate that a more crosslinked PVA hydrogel, due to the presences of higher TA, reduce ionic transport across the hydrogel thereby leading to a lower electroactivity.

On the other hand, the addition of CQDs into the PVA hydrogel (PVA/CQD) led to an increase in CV area and peak oxidation current (Fig. 3c). Moreover, increasing amounts of CQDs into the hydrogel increased both these parameters

leading to a general improvement in the electroactivity of the PVA hydrogel with a maximum SC of 0.17 mF g^{-1} with PVA/CQD-0.04. Similar SC increase to the PVA/TA system was obtained, but using a much less amount of active material due to its large electroactivity.

Swelling Ratio Effect

The swelling properties of PVA composites using independent additives placed in PBS solution (pH 7.4) for 7 days were shown in Fig. 4. The results show that addition of the PEDOT:PSS into the PVA hydrogel (PVA/PEDOT) led to an increase in the SR of the PVA hydrogel. In fact, a higher content of PEDOT:PSS (PVA/PEDOT-0.65) increased the SR of the pristine PVA hydrogel (SR = 823%) up to SR = 918% (Fig. 4a).

On the other hand, the addition of TA to the PVA hydrogel led to a generalized decrease in the SR up to ΔSR = − 200% in the PVA/TA-1 hydrogel (Fig. 4b). This behavior could be expected, as TA results in a more crosslinked and more compact PVA hydrogel, thus strengthening the internal hydrogen bond network of the PVA matrix. This also might explain the reduction in the SC observed at higher TA concentration in the PVA/TA hydrogel. However, more deep insight has to be conducted on the mechanical properties and hydrogel morphology to extract conclusions.

The results of the 7-day SR tests of the CQD hydrogels show also a tendency to increase the SR with the presence of CQDs in the sample except for the lowest

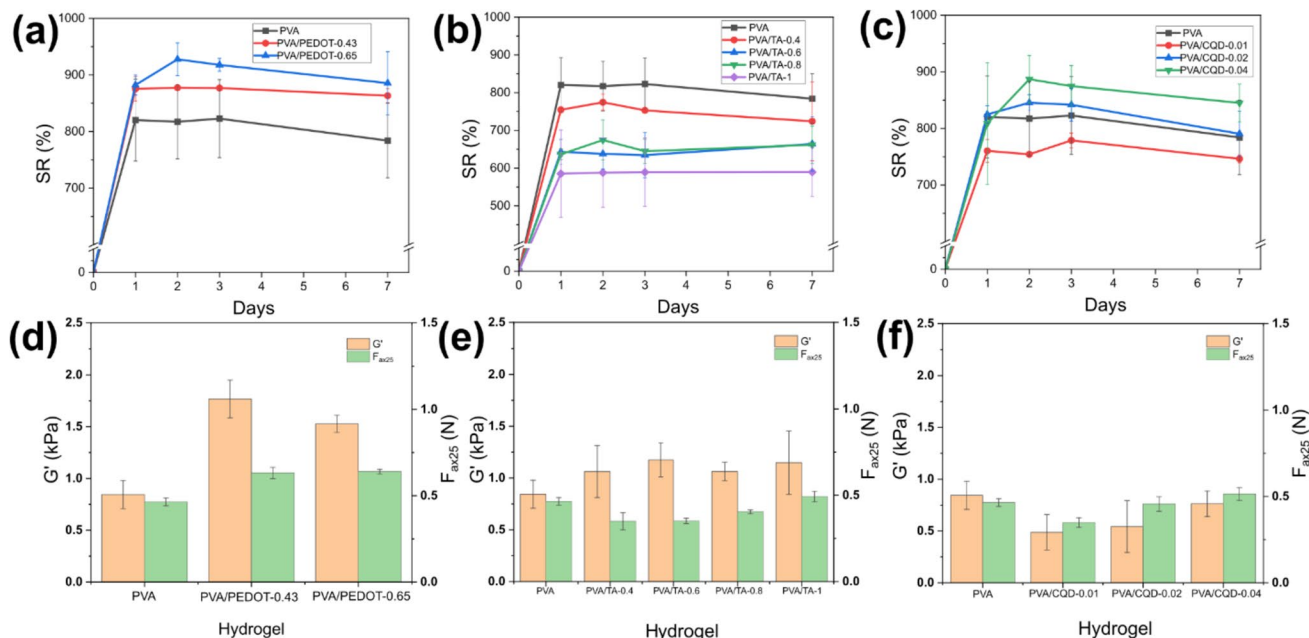**Fig. 4** 7-day swelling ratio (SR), storage modulus (G', orange squares) and axial compression force (F$_{ax25}$, green squares) of **a**, **d** PVA/PEDOT, **b**, **e** PVA/TA, and **c**, **d** PVA/CQD hydrogels at different concentrations of additives

concentration (PVA/CQD-0.01) of CQDs (Fig. 4c). As seen in the figure, the lowest concentration of CQDs resulted in a 50% reduction in swelling ratio, while higher concentrations led to an increase in SR. However, as the SR values are quite close to each other, as shown by the standard deviation bars, these differences of 50% could be due to measurement errors and inhomogeneous dispersion of CQDs when using such low concentrations. Since the samples were in the range of 50 to 100 mg, slight differences in the measurements cause large deviations in the calculations.

Mechanical Effect

Oscillatory rheological experiments were conducted in all PVA based composites hydrogels using PEDOT:PSS, TA and CQD as individual additives, to determine their storage modulus (G') and the axial compression force (F_{ax25}) required to induce a 25% deformation on the studied hydrogels samples.

The addition of the PEDOT:PSS into the PVA hydrogel led to an increase both the F_{ax25} and G' mechanical properties (Fig. 4d). More specifically, G' and F_{ax25} increased up to 111% and 37%, respectively, compared to the values of pristine PVA hydrogel when PEDOT:PSS (PVA/PEDOT-0.43) was added. The addition of PEDOT:PSS into the PVA polymer chain reinforce inter-chain interaction by forming additional hydrogen bonding between sulfonic groups of PSS and the hydroxyl groups of PVA [36]. A subsequent increase on the content of PEDOT:PSS (PVA/PEDOT-0.65) did not affect the F_{ax25} but did decrease G' a little bit, which shows that the PEDOT:PSS improves the elasticity of the PVA hydrogel. The effect of TA addition on the mechanical properties of the PVA hydrogels is observed in Fig. 4e. The addition of TA leads to an increase in G', demonstrating an improvement in elasticity without reaching the final values previously obtained with the PEDOT:PSS additive. On the other hand, the F_{ax25} seems to have decreased slightly with the addition of TA, likely due to the inter-chain cohesive forces that TA is exerting. The results do not show a great improvement in the mechanical properties with the addition of TA, as expected, although a greater difficulty is observed in water infiltration into the hydrogel matrix for its swelling.

The addition of the CQDs appears to slightly decrease the F_{ax25} of the PVA hydrogel, showing a possible increase in the softness of the hydrogel (Fig. 4f). On the other hand, the addition of the CQDs does not seem to have a clear effect on G'. These results show that the CQDs may not have an effect on the mechanical properties of the PVA hydrogel, at these very low concentrations.

Multi-additive PVA-Based Hydrogels

Based on the results of the effects on electroactivity and mechanical properties of the individual components on the PVA hydrogel, specific additive values were chosen. As the addition of the CQDs did not seem to enhance the mechanical properties of the PVA hydrogel, the composition of PVA/CQD-0.04 was chosen based on its enhancement of electroactivity. On the other hand, increasing TA concentrations led to a decrease in the electroactivity of the PVA hydrogel but an increase in G' values. Hence, the composition of PVA/TA-0.4 with the highest SC value was chosen as a compromise between mechanical and electrochemical properties. Finally, the addition of PEDOT:PSS enhanced both mechanical and electrochemical properties. Although a higher concentration of PEDOT:PSS seemed to indicate a slightly weaker hydrogel, based on a lower G' value, the composition of PVA/PEDOT-0.65 was chosen based on its higher enhancement of electroactivity. For the fabrication of the hybrid hydrogels, TA was added to all the hydrogels as the additive for mechanical property enhancement, while CQDs and PEDOT:PSS were used as the electroactivity enhancers. Hence, the two-component hybrid hydrogels, PVA/PEDOT/TA and PVA/CQD/TA were fabricated. A third hybrid hydrogel, PVA/PEDOT/CQD/TA, which contains all three additives, was also fabricated in order to investigate the synergistic effects of PEDOT:PSS and CQDs on the properties of the hydrogel.

Chemical and Morphological Characterization

Figure 5a shows the comparative FTIR spectra of all synthetized PVA based hydrogels with only one additive. As the majority of the hydrogel consists of PVA, the FTIR spectra show predominantly absorption peaks from the PVA (black arrows), which present the characteristic O−H stretching peak at about 3300 cm^{-1}, C−O stretching at around 1085 cm^{-1}, and asymmetric CH$_2$ stretching at around 2910 cm^{-1} [37].

For the PVA/CQD-0.04 hydrogel, the characteristic peaks exhibited by the CQDs could not be spotted within the PVA hydrogel due to the very low concentration of CQDs within the PVA hydrogel. As for the PVA/TA-0.4 hydrogel, some peaks due to the TA could be slightly seen at 1712 cm^{-1}, 1200 cm^{-1}, and 1610 cm^{-1}, attributed to the C=O stretching of the esters, C−O stretching of the esters, and C=C ring stretching, respectively [38]. However, only the peaks at 1200 cm^{-1} could be clearly observed in the PVA/TA-0.4 hydrogel. The observed results are in line with a previous work wherein some TA peaks in PVA hydrogels are only visible at higher concentrations [38].

Finally, PVA/PEDOT-0.65 hydrogel showed peaks at around 1646 cm^{-1} and 975 cm^{-1}, which was assigned to
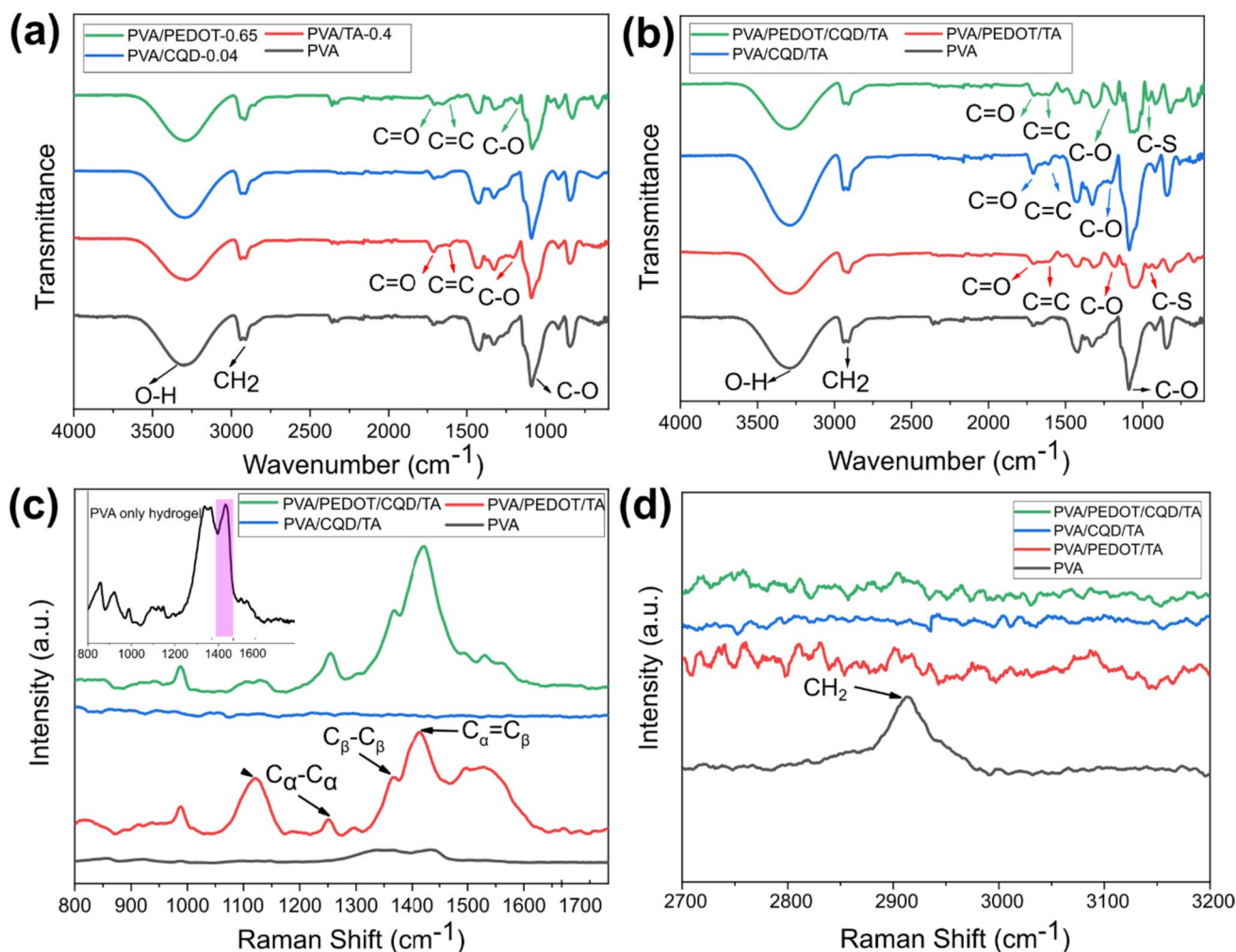
Fig. 5 FTIR spectra of **a** PVA, PVA/PEDOT-0.6, PVA/CQD-0.04, PVA/TA-0.4, and **b** hybrid PVA/PEDOT/TA, PVA/CQD/TA and PVA/PEDOT/CQD/TA hydrogels. **c** Raman spectra of hybrid hydrogels along the **c** low and **d** high Raman shift spectra

the C=C stretching vibration and C-S vibration of PEDOT, respectively [39], while the peaks at 1175 cm^{-1} and 1130 cm^{-1}, indicates sulfonic acid groups [40].

The successful incorporation of the multiple additives in the PVA hydrogels show the combination of the PVA, PEDOT:PSS, and the TA characteristic peaks in the FTIR spectra, as shown in (Fig. 5b).

Raman spectra of PVA based hydrogels are shown in Fig. 5c and d. The bands at 1430 cm^{-1} and 2910 cm^{-1} represent the characteristic peaks of PVA due to the stretching vibrations of –CH and –CH$_2$, respectively [41]. A graph of the PVA/PEDOT-0.65 hydrogel spectrum was shown separately as an inset in Fig. 5c, as the signals of this hydrogel were very weak compared to the signals of the other additives.

PEDOT has characteristic peaks at 1260, 1370, and 1450 cm^{-1} that represent the C$_\alpha$-C$_\alpha$ inter-ring stretching, C$_\beta$–C$_\beta$ stretching, and C$_\alpha$=C$_\beta$ symmetric stretching vibration,

respectively [42]. In the case of the hybrid hydrogels containing PEDOT:PSS, a strong peak was observed at the 1420 cm^{-1}, which could indicate a shift in the PEDOT peak due to its interaction with PVA. This peak is attributed to PEDOT and not to PVA because according to the previous works, combinations of PVA and PEDOT:PSS does not result in visible PVA peaks due to the intensity of the PEDOT:PSS peaks [42, 43]. Moreover, the PEDOT peaks at 1260 and 1370 cm^{-1} also show shifts to 1250 and 1365 cm^{-1}, respectively.

TA, on the other hand, has characteristic peaks at 1614 and 1712 cm^{-1} [44]. However, these peaks were not evident in any of the hydrogels possibly due to the low concentration of TA.

Unfortunately, there are no distinct peaks, even those of PVA, that can be obtained from the hybrid hydrogel containing only TA and CQDs. A hypothesis for this is the presence of the CQDs, which are fluorescent. Hence, in the

absence of a compound with an intense Raman spectrum, like PEDOT:PSS, the spectrum of the hydrogel is dominated by the fluorescent nature of the CQDs, which could suppress the Raman signal. For these samples, better Raman spectra could be obtained with near infrared lasers [45].

SEM images of the surface and cross sections of the freeze-dried hydrogels samples were taken. Hydrogel porosity was calculated by means of their cross-sectional images and using the ImageJ software. Figure 6 shows a SEM image of the different cross sections of PVA based hydrogel with multiple additives compared to pristine PVA hydrogel. As can be seen, the additives generally increase the average pore size of the pristine PVA (Fig. 6a). In addition, a greater roughness appears on the interior walls of the hydrogels containing PEDOT:PSS, observing the formation of small growths in the form of sub-meshes that could be attributed to the presence of this additive (Fig. 6b and d). The presence of CQDs also increases the macroporosity but not the roughness of the sample (Fig. 6c). Indeed, there is a wide distribution of pore sizes in all hydrogels, clearly the PVA/PEDOT/TA hydrogel (Fig. 6b) having the largest pore size.

Table 1 lists among other variables the averaged pore size distribution (d_p) and SR in all PVA-based hydrogel

Table 1 Averaged Pore Size (d_p, in μm), Swelling Ration (**SR**, in %), Specific Capacitance (**SC**, in mF g^{-1}), and Loss of Electroactivity (**LEA**, in %) of all hydrogels

Hydrogel	d_p (μm)	SR (%)	SC (mF/g)	LEA
PVA	2.09 ± 0.69	823 ± 69	0.13 ± 0.02	3.1 ± 0.8
PVA/TA-0.4	2.36 ± 1.09	753 ± 1	0.20 ± 0.01	4.9 ± 2.5
PVA/PEDOT-0.65	3.41 ± 1.38	918 ± 11	0.50 ± 0.04	-3.1 ± 2.7
PVA/CQD-0.04	3.41 ± 1.53	875 ± 36	0.17 ± 0.06	8.1 ± 3.3
PVA/PEDOT/TA	3.49 ± 1.68	808 ± 87	0.29 ± 0.06	3.6 ± 0.9
PVA/CQD/TA	2.32 ± 0.95	812 ± 22	0.47 ± 0.05	3.2 ± 1.7
PVA/PEDOT/CQD/ TA	2.75 ± 1.15	966 ± 25	0.39 ± 0.04	5.9 ± 0.3

systems. It is observed that all the additives independently tend to increase the pore size, although TA does so to a lesser extent. It is interesting to note that the addition of TA to the PVA/CQD (PVA/CQD/TA) hydrogel results in a small reduction in the mean pore size, although it does not appear to affect the PVA/PEDOT system. On the other hand, taking into account the SR of the different systems studied, TA not only decreases the swelling of PVA due to the crosslinking reinforcement of the polymeric matrix
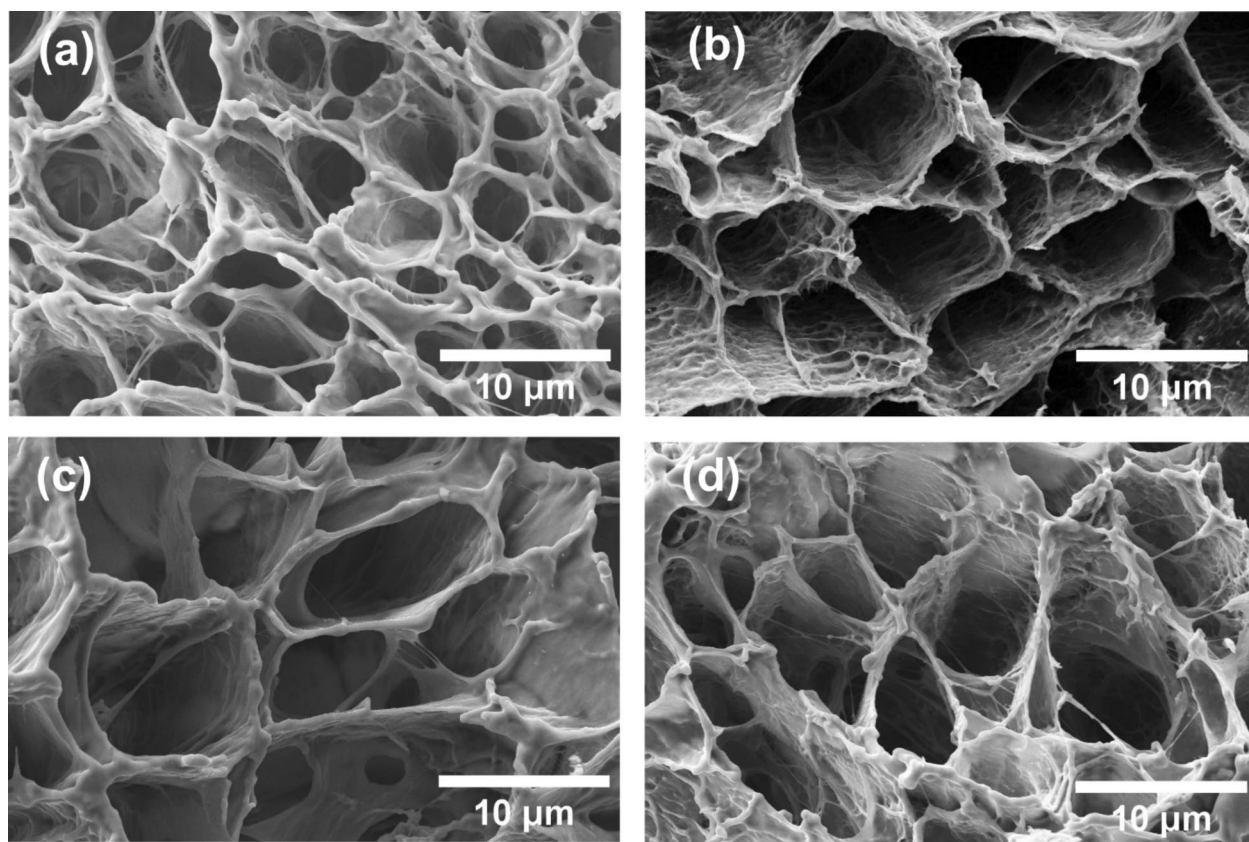

Fig. 6 Cross-sectional SEM images of freeze-dried hydrogels. Representative SEM images of **a** PVA hydrogel; **b** PVA/PEDOT/TA hydrogel; **c** PVA/CQD/TA hydrogel; **d** PVA/PEDOT/CQD/TA. Micrographs recorded with 3000x magnifications are displayed

(PVA/TA hydrogel), but also partially counteracts the swelling produced by the PEDOT:PSS and CQDs additives in their hybrid hydrogels.

The swelling properties in hybrid PVA composites using multiple additives placed in PBS solution (pH 7.4) for 7 days were shown in Fig. 7a. The results show that PVA/PEDOT/TA and PVA/CQD/TA hybrid hydrogels resulted in a similar SR compared to pristine PVA hydrogel. This is in line with the previous SR results for additives independently added to PVA, where PEDOT:PSS and CQDs increased SR while TA reduced it, leading to a similar SR values to that of PVA hydrogel. On the other hand, PVA/PEDOT/CQD/TA hydrogel, which contained the three additives, resulted in a significant increase in SR compared to the PVA hydrogel, more than compensating for the opposite effect of TA on the material.

A separate study of the swelling ratio of the PVA and hybrid hydrogels were conducted in the first 24 h (Figure S2). The results show a rapid swelling of the hydrogels within the first hour, exhibiting the steepest slope of the curve. Within the first hour, the PEDOT-containing hydrogels (PVA/PEDOT/TA and PVA/PEDOT/CQD/TA) exhibited a swelling ratio of up about 470%. The PVA hydrogel was slower, reaching up to about 405%. While the PVA/CQD/TA hydrogel had the slowest swelling, reaching about 350% within the first hour. While the hydrogels continued to swell along the 24 h, the steep of the curve gradually decreases, almost reaching a plateau between the 20th and 24th hour. As shown in the long-term experiments, the swelling ratios of the hydrogels were consistent up to the third day, after which a gradual decrease in SR is observed.

Mechanical Properties

Oscillatory rheological experiments were conducted in all hybrid PVA composites hydrogels (Fig. 7a) to determine G' and F_{ax25} mechanical properties. The mixture of the PEDOT:PSS and TA led to a large increase in the G' and F_{ax25}. Similar to what was observed when both additive where added independently to the pristine PVA hydrogel. On the other hand, the combination of TA and CQDs only led to a slight increase in both, although more accentuated for the F_{ax25} values. When all three additives are combined together, the mechanical properties were improved compared to the PVA hydrogel but are lower compared to the hydrogel with both PVA/PEDOT and PVA/TA hydrogels, which could show that the addition of the CQDs led to a decrease in the mechanical properties. This is in line with the result of the CQDs only hydrogels (PVA/CQD, Fig. 4).

Electrochemical Characterization

Figure 8a show CVs of the PVA and selected hybrid hydrogels. In all the hybrid hydrogels, the shape of the CV curve changes from a symmetric box-like shape into an asymmetric curve with a peak at around 1 V. This change in shape is also accompanied by an increase in the area of the CV curve. The highest peak current was obtained from the PVA/CQD/TA, followed by the PVA/PEDOT/CQD/TA, and finally the PVA/PEDOT/TA hydrogels.

Table 1 also lists SCs of the hybrid hydrogels, after soaking the hydrogels in PBS overnight. It is observed that all hybrid hydrogels lead to at least twice the SC and at best four times the SC, compared to bare PVA hydrogel. Moreover, considering only the hybrid hydrogels with multiple
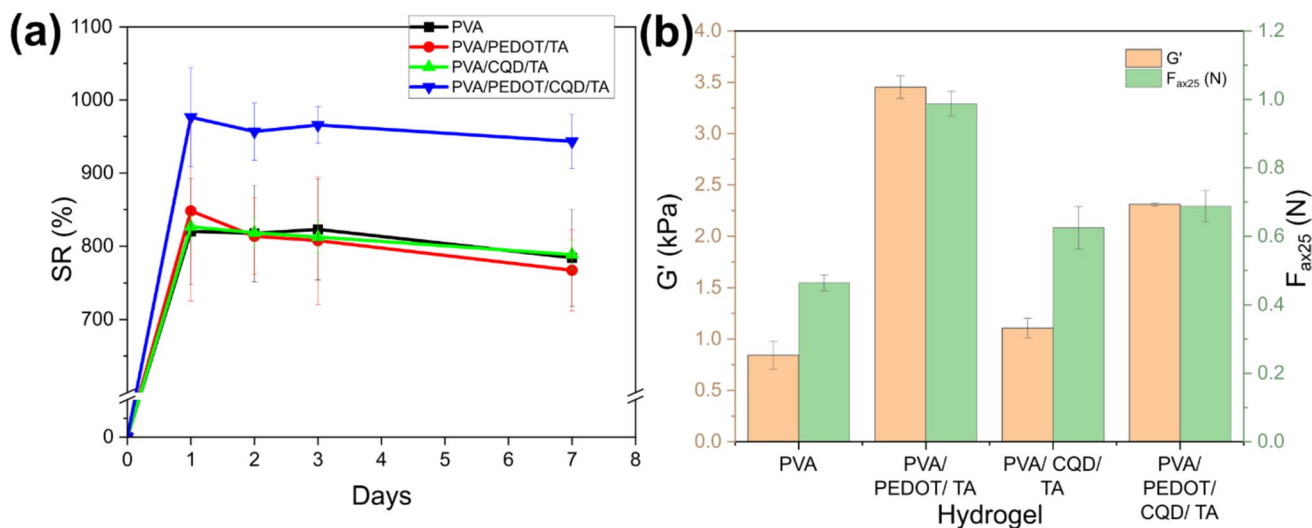

Fig. 7 **a** Swelling ratio (SR), and **b** Storage modulus (G') and axial compression force (F_{ax25}) of the PVA-based hybrid hydrogels
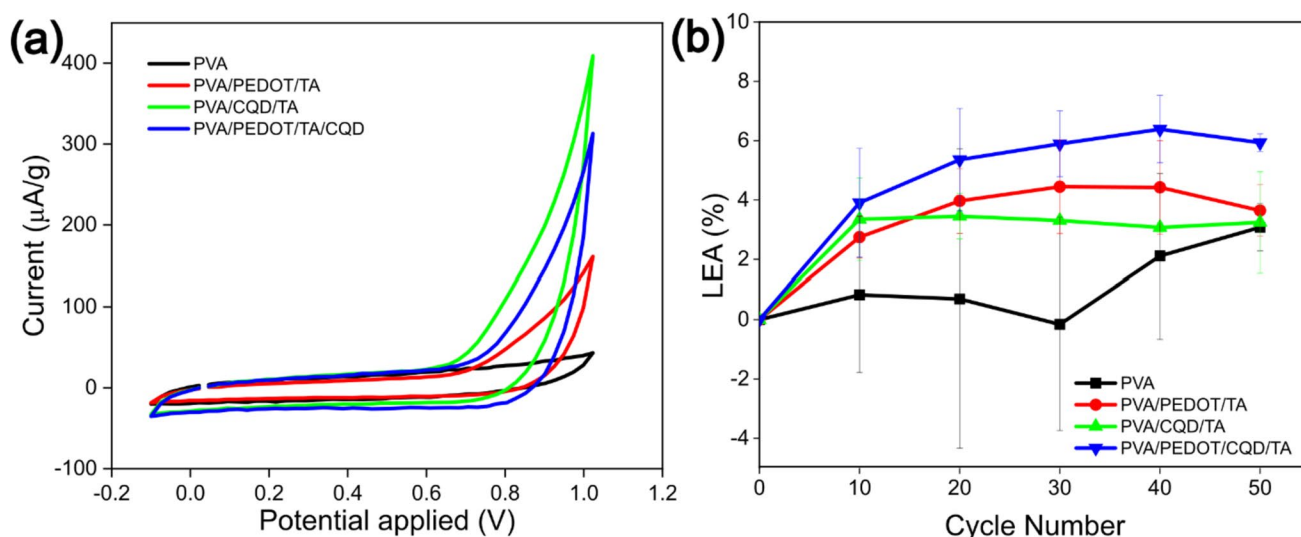
Fig. 8 **a** Cyclic voltammograms at cycle 3 and **b** Loss of Electroactivity (LEA, %) for PVA, PVA/PEDOT/TA, PVA/CQD/TA and PVA/PEDOT/CQD/TA hydrogels. Voltammograms were obtained at the scan rate of 50 mV s^{-1} using PBS buffer solution

additives, the combination of CQDs and TA (PVA/CQD/TA) led to the highest SC in accordance with Fig. 8a, followed by the combination of all three additives. Surprisingly, the combination of PEDOT:PSS and TA (PVA/PEDOT/TA) generated the lowest specific capacitance. The synergistic effect of combined additives on hydrogels are behind the observed properties. Indeed, these results suggest that TA enhances the electroactivity of CQDs but reduces that of PEDOT:PSS in the final hydrogels. The presence of TA could be interfering within the conducting pathway of the PEDOT:PSS within the hydrogel matrix, hence leading to a lower electroactivity. On the other hand, the enhancement of electroactivity in the presence of both CQDs and TA could be due to the intrinsic electroactivity of each additive and as well as the possible interactions between these two. Both TA

and CQDs have the ability to form hydrogen bonds with the PVA chains and possibly with each other in the PVA/CQD/TA hydrogel (Fig. 9). This interaction could hence improve the CQDs retention within the PVA/CQD/TA hydrogel, which could explain the lower LEA of the PVA/CQD/TA hydrogel of 3.2% compared to the LEA of the PVA/CQD-0.04 hydrogel of about 8.1%. This could be explained by the interaction forming between TA and CQD. This interaction was the basis of some fluorescent-based sensing of TA, wherein the presence of TA in a sample quenches the fluorescence of CQDs [46, 47].

Figure 8b shows the progression in the LEA of the PVA and hybrid hydrogels along 50 CV cycles. For the three hybrid hydrogels, the steepest part of the curve occurs between 0 and 10 CV cycles, after which the graph occurs,

Fig. 9 Scheme of the main hydrogen bond interactions within the PVA/CQD/TA hydrogel matrix
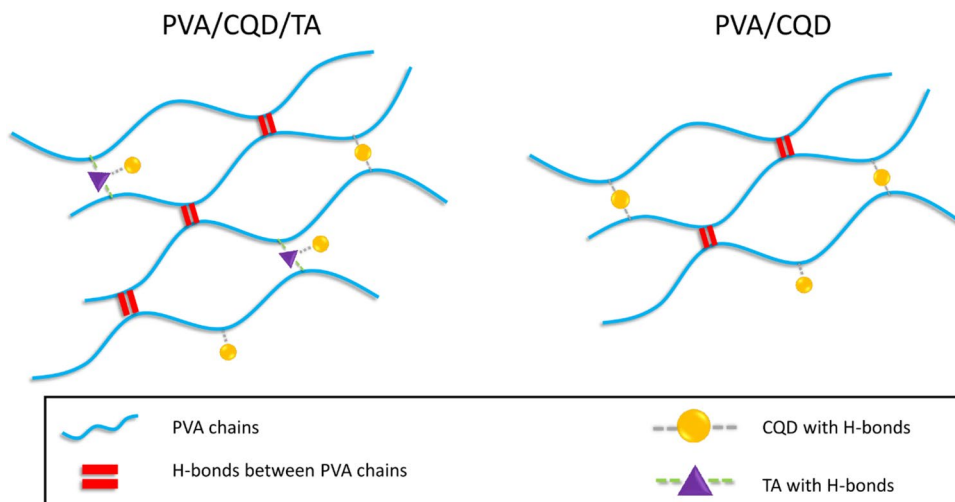
indicating a stabilization of the electroactivity of the hydrogel. The PVA/PEDOT/CQD/TA hydrogel demonstrated the highest loss in electroactivity at 5.9%, while the PVA/CQD/TA and PVA/PEDOT/TA hydrogels showed very close LEA at 3.6% and 3.2%, respectively. On the other hand, the PVA only hydrogel shows a fairly stable electroactivity, with the lowest LEA of only 3% after 50 cycles. Indeed, all the samples show a very low LEA. Interesting to notice that the combination of both PEDOT:PSS and CQDs accentuated the loss in electroactivity.

The progression of the CV curves for the hybrid and PVA hydrogels from cycle 3 to 50 are shown in the ESI (Figure S3). The results show a good stability across the 50 cycles for all of the hydrogels. There is a slight decrease in the intensity of the anodic peak at around 1 Vafter 50 cycles, indicatings a quasi-reversible behavior, as only a small fraction of the hydrogel electroactivity is lost or irreversibly degraded due to overoxidation. Moreover, the loss of electroactivity is directly proportional to the increase in redox cycles applied, suggesting that as the least stable part of the structure degrades, the system gradually "aged" by redox cycles which tends to 100% reversible behavior. It can also be observed the recorded voltammetric curves have increasing values of anodic intensity as they approach 1 V. This intensity peak reveals a clear tendency of the system to form electroactive polarons (and perhaps also bipolarons) around the indicated potential and in the case of hybrid hydrogels, the tendency for this phenomenon to occur increases notably with the addition of tannic acid to the hydrogel. This is evident in Fig. 3b, where the PVA/TA-1 (the sample with the highest TA content) presented a strong peak at around 1 V. Although the system does present asymmetric redox cycles, this does not diminish their electrochemical reversibility.

Finally, electrochemical impedance spectroscopy (EIS) was performed on the hydrogels, showing the electronic conductivity provided by the additives to the hydrogels (Figure S4). The Nyquist graphs obtained for all the hydrogels show a semicircle followed by an almost vertical straight line. The results show that the addition of the PEDOT:PSS into the hydrogel resulted in an improvement in the conductivity, as evidenced by the reduction in the semicircle. A slight increase in the semicircle radius was obtained upon the addition of TA into the system (PVA/PEDOT/TA) and a further slight increase upon the addition of CQD (PVA/PEDOT/CQD/TA). The Nyquist plots of the PEDOT-containing hydrogels all exhibit a lower semicircle radii compared to the PVA hydrogel, demonstrating an improvement in conductivity. On the other hand, the PVA/CQD/TA hydrogel has almost the same semicircle radius as the PVA hydrogel. This could indicate an improvement in the capacitive behavior of hydrogel with the combination of CQD and TA, as exhibited by these hydrogels having the highest specific capacitance calculated from CV results.

Degradation Study

The hydrogel degradation test was performed on all PVA-based composites in two different steps. First, considering the effect of a single additive on degradation by measuring the loss of mass at the end of 7 days in PBS solution under constant agitation. Second, by measuring the synergistic effect of more than one additive on the degradation of PVA hydrogels based on mass and SC loss over 56 days (8 weeks).

Figure S5a shows the degradation of the PEDOT:PSS hydrogels after 7 days. It was observed that the addition of PEDOT:PSS to the hydrogel led to increased degradation of the pristine PVA. This was expected due to the increase in pore size and SR that this additive induces to the PVA hydrogel. However, it is interesting to note that the hydrogel with the lower PEDOT:PSS content (PVA/PEDOT-0.43) showed slightly higher degradation compared to the hydrogel with the highest PEDOT:PSS content (PVA/PEDOT-0.65). The degradation test at growing amounts of TA (Figure S5b) shows a large increase in the degradation of the hydrogels upon the addition of TA. Moreover, there is a slight upward trend in degradation with respect to increasing TA content. This increase in degradation rate of the PVA hydrogel with TA could be due to the release of TA from the hydrogel, which leads not only to a decrease in weight due to loss of TA but also to the breakdown of the PVA hydrogel, as TA is intertwined within the PVA chains. This release of TA could be due to the dissolution of TA or to the oxidation of TA in the presence of PBS [48]. The degradation of PVA/CQD hydrogels containing different concentrations of CQDs is shown in Figure S5c. From the results it was possible to observe how the addition of CQDs also led to an increase in the degradation of the PVA hydrogel. The structural changes that this additive induces in the PVA hydrogel favor its degradation by increasing its porosity and SR. However, the –COOH, –NH and –OH groups observed on the surface of the CQDs have the ability to form hydrogen bonds with the PVA chains (Fig. 9), thus hiding the surface polar groups of PVA to its solvent exposure, slowing down the rate of degradation when increase the concentration of CQDs. Unfortunately, during the degradation process, the CQDs are easily released favoring the degradation of the PVA hydrogels. The use of additional linkers that fix the CQDs to the PVA hydrogel matrix would help to reduce the solvent exposure. TA and CQDs are reinforcing the hydrogel network by means of hydrogen bonds, which increase their mechanical properties. However, the easy loss of TA and CQD observed during the material degradation (which are acting as physical cross-linker), accelerate the DR. From greatest to least effect of the additive on the DR increase are TA > CQD > PEDOT:PSS.

Additionally, a further degradation study of several PVA-based hydrogels with multiple additives was performed. Figure 10 shows the 8-week mass and SC loss evolution of the hybrid hydrogels in a PBS solution under constant agitation. As shown in Fig. 10a, all additives led to an increase in the degradation of the pristine PVA hydrogel. The mass losses of the PVA and PVA/CQD/TA hydrogels seem to have stabilized after the first week, reaching about 15% and 25% of DR after the 8-week test, respectively. On the other hand, the degradation of the PVA/PEDOT/TA and PVA/PEDOT/CQD/TA hydrogels stabilized after the second week, reaching about 22% and 29% of DR at the end of the test, respectively. All the additives used have shown an amplifying effect of the DR with respect to the pristine PVA hydrogel, which would explain the highest DR was reached in the PVA/PEDOT/CQD/TA hydrogel. Observed DR increases compared to that of the pristine PVA hydrogel could be the result of the dissolution, release, or oxidation of the additives, leading to a breakdown of the PVA hydrogel network. Along with an 8-week test the SC was also obtained to monitor the electroactivity loss due to the degradative process (Fig. 10b). All hybrid hydrogels remained stable until week 2, after which the SC values dropped to similar values to those of pristine PVA hydrogel. This is mainly due to the degradation of the hydrogel as a whole, as per the mass loss data, and also to the loss of electroactivity of the additives. The PVA/PEDOT/CQD/TA hydrogel is the one that kept the highest overall electroactivity throughout the 8 weeks with a slower decrease in SC. Interestingly, lost in electroactivity test results (Fig. 8b) follows a fairly similar trend to the DR results, wherein the PVA/PEDOT/CQD/TA hydrogel exhibited the highest LEA after 50 CV cycles, while the PVA only hydrogel exhibited the lowest. Hence,

some type of relationship could be established between the loss in electroactivity and the degradation of the hydrogels.

PVA-Based Hydrogels as Potential Pressure Sensor

Conductive hydrogels can have the potential for use as pressure and strain sensors, as changes in their conformation could disrupt the conducting pathways inside the hydrogels, leading to changes in the overall conductivity of the material. Indeed, PVA-based hydrogels have been used as pressure or strain sensors [49–53]. Hence, the use of these hybrid hydrogels as pressure sensors was evaluated by testing the two PVA-based hydrogels obtained with multiple additives and containing CQDs that exhibited the highest electroactivity, i.e., PVA/CQD/TA and PVA/PEDOT/CQD/TA. The sensor was built using a sandwiched configuration, in which each hydrogel piece was arranged separating two ITO-coated PET sheets at a distance of 3 mm as described in the Methods section. To obtain the signals associated to pressure variation, the sensor was integrated in an Arduino circuit (Fig. 11a) and the relative resistance change ($\Delta R/R0$) over time in a cyclic weighing exposure was measured. The tested hydrogels were subjected to constant pressures of 12.8 and 25.7 kPa for the PVA/CQD/TA and PVA/PEDOT/CQD/TA hydrogels, respectively. The applied pressure and relaxation cycles were repeated every $10+10$ s throughout the test. Figure 11b shows the relative resistance change of the two sensors over five cycles without rehydration of the material. The shapes of the relative resistance changes for both hydrogels were quite similar. Upon the application of pressure, there was a steep drop in the resistance. The response time of the hydrogels to this pressure application was less than 400 ms. Upon pressure removal, there was a sudden
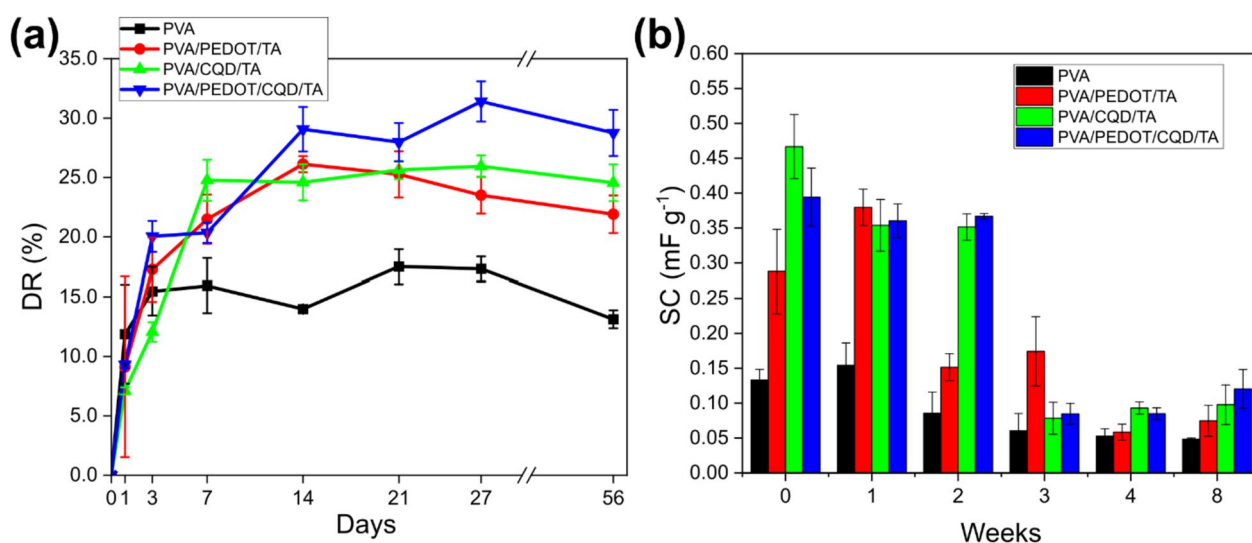

Fig. 10 8-week degradation study of the hybrid hydrogel: **a** degradation rate (DR, %) and **b** specific capacitance evolution (SC, mF g^{-1})
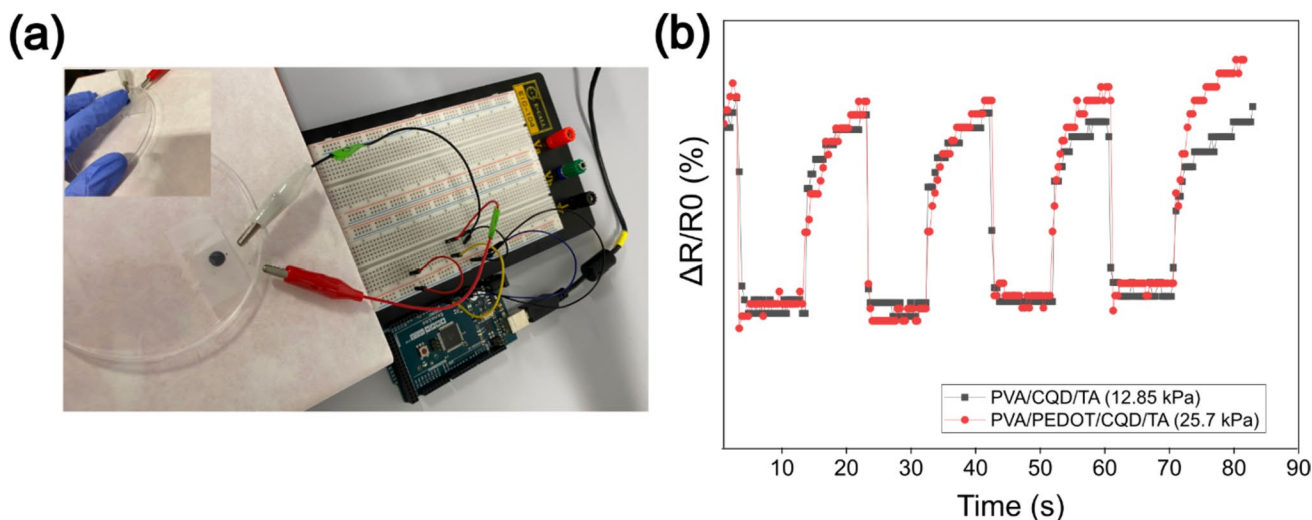
Fig. 11 Pressure response of hybrid PBA-based hydrogels. **a** Set up used for constant and cyclic pressure measurements; **b** Relative resistance change ($\Delta R/R_0$, %) of hydrogels subjected to different cyclic pressures PVA/CQD/TA (12.8 kPa) and PVA/PEDOT/CQD/TA (25.7 kPa)

increase in the resistance, followed by a plateau increase in the resistance to its original pre-pressure resistance value. This behavior was repeated upon multiple cycles of pressure application, demonstrating that the response of the hybrid hydrogels was constant throughout the test.

The PVA/PEDOT/CQD/TA hydrogel showed unstable and erratic responses in previous tests performed at lower pressures (Figure S6). Indeed, the PVA/PEDOT/CQD/TA hydrogel was much less sensitive to pressure changes, requiring twice the pressure to induce a similar resistance change compared to the PVA/CQD/TA hydrogel to obtain similar response. In addition, the increase in electric resistance upon pressure removal was not as steep in the PVA/PEDOT/CQD/TA hydrogel compared to the PVA/CQD/TA hydrogel. Rather, upon pressure removal the PVA/PEDOT/CQD/TA hydrogel seemed to undergo a sudden but slight relaxation, followed by a slow return to its non-compressed state, as indicated by its shorter steep jump and a longer recovery region. The behavior differences between the two hydrogels can be directly attributed to the presence or absence of PEDOT:PSS as an additive. As demonstrated above, the addition of PEDOT:PSS resulted in stiffer hydrogels. Specifically, the storage modulus of the PVA/CQD/TA and PVA/PEDOT/CQD/TA hydrogels used in the sensor were 1.11 and 2.31 kPa, respectively. Stiffer hydrogels require higher pressures to exhibit any noticeable conformational and, in turn, resistance changes within the 3D lattice of the hydrogel. Therefore, this could explain the higher pressure needed to induce the same relative resistance change to the PVA/PEDOT/CQD/TA hydrogel compared to the PVA/CQD/TA hydrogel. Similarly, a stiffer and less resilient hydrogel might require more time to return to its original state when any external forces are removed. This is in line to the slower recovery rate observed of the hybrid hydrogel containing PEDOT:PSS. Furthermore, the rehydration factor here plays an important role in the long time behavior of the hydrogel. In fact, it can be observed how the baseline of Fig. 11b presents an upward drift as the pressure-relaxation cycles occur due to the internal change of the hydrogel structure, mainly due to the expulsion of internal electrolyte without its reposition, thus increasing its electric resistance. The drift in the baseline is greater for the PVA/PEDOT/CQD/TA hydrogel (0.09 $\Delta\%$ cycle^{-1}) than the PVA/CQD/TA hydrogel (0.05 $\Delta\%$ cycle^{-1}), which corroborates the previous observations.

The different sensitivity to pressure depending on the additives or composition of these hybrid PVA-based hydrogels could be of great interest. On the one hand, they can be used as sensors for different pressure ranges, being the hydrogels containing PEDOT:PSS (i.e., PVA/PEDOT/CQD/TA) applicable for parts of the body that suffer higher pressures, such as joints and the spine. On the other hand, the hydrogels without conducting polymer studied in this work (PVA/CQD/TA) could be applied for smaller pressure ranges, such as small muscle contractions or blood pressure. Furthermore, the PEDOT-containing hydrogels could be used as pressure-insensitive electrodes in low pressure body parts, as they are less sensitive to low pressures. These are preliminary studies that show the possibility to use these materials as sensors. Additional studies could be conducted in the future to further characterize their sensing abilities. Moreover, hydrogels based on PEDOT, PEDOT:PSS, tannic acid, carbon quantum dots, and other materials at different combinations and concentrations have already been previously studied for their use as pressure and strain sensors [50, 52, 54].

Conclusions

Nitrogen CQDs were prepared using a hydrothermal method and combined with PEDOT:PSS and TA as electroactive enhancers additives to obtain PVA-based conducting hydrogels. A study of the electroactivity and mechanical properties has been carried out for each of the additives used independently and in combination. It is observed that CQDs with a much smaller amount confer electrochemical properties similar to the other additives, so they become a very good additive to work with conducting hydrogels. Unlike the others, the TA improves the mechanical conditions of the PVA at the expense of a more compact structure and a lower SR. On the other hand, the PEDOT:PSS introduces greater stiffness and pore size to the system. In general, all the additives favor the degradation of PVA, especially the systems with PEDOT:PSS due to their greater porosity. Although the additives accelerate the degradation process of the PVA-based hydrogel, the synergistic effect of the additives helps to keep the electrochemical activity always much higher than that of the pristine PVA hydrogel during the degradation process and also delays one to two weeks the decrease in its electrochemical properties. Even so, the CQDs physically fixed to the PVA, in the degradative process are removed more quickly from the hydrogel, which could be avoided at higher concentrations using a chemical fixation. The potential use of these new PVA-based conducting hydrogels and enhanced with CQDs as pressure sensors has been successfully shown. The test carried out on two hydrogels of different stiffness demonstrated how easy it is to tune the sensitivity and range of action of these new nanomaterials based on of its composition.

Declarations

Competing Interests The authors declare no competing interests.

References

1. Ádám B, Göen T, Scheepers PTJ, Adliene D, Batinic B, Budnik LT et al (2021) From inequitable to sustainable e-waste processing for reduction of impact on human health. Environ Environ Res 194:110728

2. Forti V, Balde CP, Kuehr R, Bel G, The Global E-waste, Monitor (2020) : Quantities, flows and the circular economy potential. Bonn, Geneva and Rotterdam: United Nations University/United Nations Institute for Training and Research, International Telecommunication Union, and International Solid Waste Association; 2020

3. Li W, Liu Q, Zhang Y, Li C, He Z, Choy WCH et al (2020) Biodegradable materials and Green Processing for Green. Electron Adv Mater 32(33):2001591

4. Zhu J, Wen H, Zhang H, Huang P, Liu L, Hu H (2023) Recent advances in biodegradable electronics- from fundament to the next-generation multi-functional, medical and environmental device. Sustain Mater Technol 35:e00530

5. Ben Halima N (2016) Poly(vinyl alcohol): review of its promising applications and insights into biodegradation. RSC Adv 6(46):39823–39832

6. Adelnia H, Ensandoost R, Shebbrin Moonshi S, Gavgani JN, Vasafi EI, Ta HT (2022) Freeze/thawed polyvinyl alcohol hydrogels: Present, past and future. Eur Polym J 164:110974

7. Wan W, Bannerman AD, Yang L, Mak H (2014) Poly(Vinyl Alcohol) Cryogels for Biomedical Applications. In: Okay O (ed) Polymeric cryogels: Macroporous gels with Remarkable Properties. Springer International Publishing, Cham, pp 283–321

8. Lu J, Hu O, Hou L, Ye D, Weng S, Jiang X (2022) Highly tough and ionic conductive starch/poly(vinyl alcohol) hydrogels based on a universal soaking strategy. Int J Biol Macromol 221:1002–1011

9. Fan L, Xie J, Zheng Y, Wei D, Yao D, Zhang J et al (2020) Antibacterial, Self-Adhesive, recyclable, and tough conductive composite hydrogels for ultrasensitive strain sensing. ACS Appl Mater Interfaces 12(19):22225–22236

10. Fang H, Wang J, Li L, Xu L, Wu Y, Wang Y et al (2019) A novel high-strength poly(ionic liquid)/PVA hydrogel dressing for antibacterial applications. Chem Eng J 365:153–164

11. Li W, Lu H, Zhang N, Ma M (2017) Enhancing the properties of Conductive polymer hydrogels by freeze–thaw cycles for high-performance flexible supercapacitors ACS. Appl Mater Interfaces 9(23):20142–20149

12. Yu Y, Zhao X, Ye L (2023) A novel biocompatible wearable sensors based on poly (vinyl alcohol)/graphene oxide hydrogel with superior self-adhesion. Flex Sensit Compos Struct 309:116768

13. Zhou H, Wang Z, Zhao W, Tong X, Jin X, Zhang X et al (2021) Robust and sensitive pressure/strain sensors from solution

processable composite hydrogels enhanced by hollow-structured conducting polymers. Chem Eng J 403:126307

14. Qin Z, Zhao G, Zhang Y, Gu Z, Tang Y, Aladejana JT et al (2023) A simple and effective physical ball-milling strategy to prepare super-tough and stretchable PVA@MXene@PPy hydrogel for flexible capacitive electronics. Small 19(45):2303038

15. Zhu B, Chan EWC, Li SY, Sun X, Travas-Sejdic J (2022) Soft, flexible and self-healable supramolecular conducting polymer-based hydrogel electrodes for flexible supercapacitors. J Mater Chem C 10(40):14882–14891

16. Khodaee Z, Mazinani S, Sharif F (2022) Reduced graphene oxide-modified polyvinyl alcohol hydrogel with potential application as skin wound dressings. J Polym Res 30(1):5

17. Zhang Y, Wang F, Yu Y, Wu J, Cai Y, Shi J et al (2023) Multi-bioinspired hierarchical integrated hydrogel for passive fog harvesting and solar-driven seawater desalination. Chem Eng J 466:143330

18. Kim C-H, Azimi M, Fan J, Nagarajan H, Wang M, Cicoira F (2023) All-printed and stretchable organic electrochemical transistors using a hydrogel electrolyte. Nanoscale 15(7):3263–3272

19. Tan P, Wang H, Xiao F, Lu X, Shang W, Deng X et al (2022) Solution-processable, soft, self-adhesive, and conductive polymer composites for soft electronics. Nat Commun 13(1):358

20. Gamboa J, Paulo-Mirasol S, Estrany F, Torras J (2023) Recent progress in Biomedical Sensors based on conducting polymer hydrogels ACS. Appl Bio Mater 6(5):1720–1741

21. Molina BG, Llampayas A, Fabregat G, Estrany F, Alemán C, Torras J (2021) Electroactive interpenetrated biohydrogels as hybrid materials based on conducting polymers. J Appl Polym Sci 138(12):50062

22. Liu Q, Qiu J, Yang C, Zang L, Zhang G, Sakai E (2021) High-Performance PVA/PEDOT:PSS Hydrogel Electrode for all-gel-state flexible supercapacitors. Adv Mater Technol 6(1):2000919

23. Lu R, Zhang X, Cheng X, Zhang Y, Zan X, Zhang L (2020) Medical applications based on supramolecular self-assembled materials from tannic acid. Front Chem 8:583484

24. Jafari H, Ghaffari-Bohlouli P, Niknezhad SV, Abedi A, Izadifar Z, Mohammadinejad R et al (2022) Tannic acid: a versatile polyphenol for design of biomedical hydrogels. J Mater Chem B 10(31):5873–5912

25. Liu J, Li R, Yang B (2020) Carbon dots: a New type of Carbon-based nanomaterial with wide applications. ACS Cent Sci 6(12):2179–2195

26. Wang Y, Lv T, Yin K, Feng N, Sun X, Zhou J et al (2023) Carbon dot-based hydrogels: preparations. Prop Appl Small 19(17):2207048

27. Dave K, Gomes VG (2022) Bioresorbable poly(lactic acid) and organic quantum dot-based nanocomposites: luminescent scaffolds for enhanced osteogenesis and real-time monitoring. J Nanostructure Chem 12(5):951–962

28. Singh A, Qu Z, Sharma A, Singh M, Tse B, Ostrikov K et al (2023) Ultra-bright green carbon dots with excitation-independent fluorescence for bioimaging. J Nanostructure Chem 13(3):377–387

29. Paulo-Mirasol S, Izquierdo C, Alemán C, Armelin E, Torras J (2023) Flexible electrode based on nitrogen carbon quantum dots for dopamine detection. Appl Surf Sci 626:157241

30. Karimzadeh Z, Mahmoudpour M, Rahimpour E, Jouyban A (2022) Nanomaterial based PVA nanocomposite hydrogels for biomedical sensing: advances toward designing the ideal flexible/wearable nanoprobes. Adv Colloid Interface Sci 305:102705

31. Bannerman AD, Li X, Wan W (2017) A 'degradable' poly(vinyl alcohol) iron oxide nanoparticle hydrogel. Acta Biomater 58:376–385

32. Aregueta-Robles UA, Martens PJ, Poole-Warren LA, Green RA (2018) Tailoring 3D hydrogel systems for neuronal encapsulation in living electrodes. J Polym Sci Part B: Polym Phys 56(4):273–287

33. Li Z, Hu K, Li Z, Li C, Deng Y (2023) Polypyrrole-stabilized polypeptide for eco-friendly supercapacitors. Int J Mol Sci 24(3):2497

34. Sun L, Zhang H, Wang Y, Xiong Z, Zhao X, Xia Y (2021) Chitosan-derived N-doped carbon dots for fluorescent determination of nitrite and bacteria imaging Spectrochim Acta. Part A 251:119468

35. Hu M, Gu X, Hu Y, Deng Y, Wang C (2016) PVA/Carbon dot nanocomposite hydrogels for simple introduction of Ag nanoparticles with enhanced antibacterial activity. Macromol Mater Eng 301(11):1352–1362

36. Tseng Y-T, Lin Y-C, Shih C-C, Hsieh H-C, Lee W-Y, Chiu Y-C et al (2020) Morphology and properties of PEDOT:PSS/soft polymer blends through hydrogen bonding interaction and their pressure sensor application. J Mater Chem C 8(18):6013–6024

37. Kharazmi A, Faraji N, Mat Hussin R, Saion E, Yunus WMM, Behzad K (2015) Structural, optical, opto-thermal and thermal properties of ZnS–PVA nanofluids synthesized through a radiolytic approach. Beilstein J Nanotechnol 6:529–536

38. Hong KH (2017) Polyvinyl alcohol/tannic acid hydrogel prepared by a freeze-thawing process for wound dressing applications. Polym Bull 74(7):2861–2872

39. Peng Y, Yan B, Li Y, Lan J, Shi L, Ran R (2020) Antifreeze and moisturizing high conductivity PEDOT/PVA hydrogels for wearable motion sensor. J Mater Sci 55(3):1280–1291

40. Wang X, Feng G-y, Ge M-q (2017) Influence of ethylene glycol vapor annealing on structure and property of wet-spun PVA/PEDOT:PSS blend fiber. J Mater Sci 52(12):6917–6927

41. Shi Y, Xiong D, Li J, Wang K, Wang N (2017) In situ repair of graphene defects and enhancement of its reinforcement effect in polyvinyl alcohol hydrogels. RSC Adv 7(2):1045–1055

42. Kumar S, Rai P, Sharma JG, Sharma A, Malhotra BD (2016) PEDOT:PSS/PVA-Nanofibers-decorated Conducting Paper for Cancer Diagnostics. Adv Mater Technol 1(4):1600056

43. Shi W, Wang Z, Song H, Chang Y, Hou W, Li Y et al (2022) High-sensitivity and Extreme Environment-resistant sensors based on PEDOT:PSS@PVA Hydrogel fibers for physiological monitoring. ACS Appl Mater Interfaces 14(30):35114–35125

44. Wahyono T, Astuti DA, Gede Wiryawan IK, Sugoro I, Jayanegara A (2019) Fourier Transform Mid-infrared (FTIR) Spectroscopy to identify tannin compounds in the panicle of Sorghum Mutant Lines IOP conf ser. Mater Sci Eng 546(4):042045

45. Zhang Z-M, Chen S, Liang Y-Z, Liu Z-X, Zhang Q-M, Ding L-X et al (2010) An intelligent background-correction algorithm for highly fluorescent samples in Raman spectroscopy. J Raman Spectrosc 41(6):659–669

46. Yang P, Zhu Z, Chen M, Zhou X, Chen W (2019) Microwave-assisted synthesis of polyamine-functionalized carbon dots from xylan and their use for the detection of tannic acid Spectrochim Acta. Part A 213:301–308

47. Yang H, He L, Pan S, Liu H, Hu X (2019) Nitrogen-doped fluorescent carbon dots for highly sensitive and selective detection of tannic acid Spectrochim Acta. Part A 210:111–119

48. Chariyarangsitham W, Krungchanuchat S, Khuemjun P, Pilapong C (2021) Effect of advanced oxidation and amino acid addition on antioxidant capability, iron chelating property and anti-cancer activity of tannic acid. Arab J Chem 14(9):103312

49. Zhao W, Zhang D, Yang Y, Du C, Zhang B (2021) A fast self-healing multifunctional polyvinyl alcohol nano-organic composite hydrogel as a building block for highly sensitive strain/pressure sensors. J Mater Chem A 9(38):22082–22094

50. Shen Z, Zhang Z, Zhang N, Li J, Zhou P, Hu F et al (2022) High-Stretchability, Ultralow-Hysteresis ConductingPolymer

Hydrogel Strain Sensors for Soft machines. Adv Mater 34(32):2203650

51. Cao J, Zhang Z, Li K, Ma C, Zhou W, Lin T et al (2023) Self-Healable PEDOT:PSS-PVA nanocomposite hydrogel strain sensor for human. Motion Monit Nanomaterials 13(17):2465

52. Patel DK, Ganguly K, Dutta SD, Patil TV, Lim K-T (2022) Multifunctional hydrogels of polyvinyl alcohol/polydopamine functionalized with carbon nanomaterials as flexible sensors. Mater Today Commun 32:103906

53. Wang Z, Cheng F, Cai H, Li X, Sun J, Wu Y et al (2021) Robust versatile nanocellulose/polyvinyl alcohol/carbon dot hydrogels for biomechanical sensing. Carbohydr Polym 259:117753

54. Miao L, Wang X, Li S, Tu Y, Hu J, Huang Z et al (2022) An Ultra-stretchable Polyvinyl Alcohol Hydrogel Based on tannic acid modified Aramid nanofibers for Use as a. Strain Sens Polym 14(17):3532

Authors and Affiliations

Jillian Gamboa[1,2] · **Sofia Paulo-Mirasol**[1,2] · **Albert Espona-Noguera**[2,3] · **Hamidreza Enshaei**[1,2] · **Sergi Ortiz**[1] · **Francesc Estrany**[1,2] · **Maria-Pau Ginebra**[2,3] · **Juan Torras**[1,2]

✉ Juan Torras
joan.torras@upc.edu

1 Departament d'Enginyeria Química, EEBE, Universitat Politècnica de Catalunya, Av. Eduard Maristany, 10-14, Barcelona 08019, Spain

2 Barcelona Research Centre for Multiscale Science and Engineering, Universitat Politècnica de Catalunya, Av. Eduard Maristany, 10-14, Ed. I, basement, Barcelona 08019, Spain

3 Biomaterials, Biomechanics and Tissue Engineering Group, Department of Materials Science and Engineering and Research Centre for Biomedical Engineering, Universitat Politècnica de Catalunya, Av. Eduard Maristany 10-14, Barcelona 08019, Spain